Clin Exp Metastasis (2013) 30:225–236
DOI 10.1007/s10585-012-9530-0

RESEARCH PAPER

A micro-imaging study linking bone cancer pain with tumor growth and bone resorption in a rat model

Louis Doré-Savard · Nicolas Beaudet · Luc Tremblay · Yongjun Xiao · Martin Lepage · Philippe Sarret

Received: 31 January 2012 / Accepted: 21 August 2012 / Published online: 6 September 2012

Abstract Bone metastases represent a frequent complication of advanced breast cancer. As tumor growth-induced bone remodeling progresses, episodes of severe pain and fractures of weight-bearing limbs increase. All of these skeletal-related events influence the patient's quality of life and survival. In the present study, we sought to determine whether some of these pain-related behaviors could be directly correlated to tumor progression and bone remodeling. For this purpose, we used a rat model of bone cancer pain based on the implantation of mammary carcinoma cells in the medullary cavity of the femur. The bone content and tumor growth were monitored over time by magnetic resonance imaging (MRI) and micro X-ray computed tomography (μCT). The same animals were evaluated for changes in their reflexive withdrawal responses to mechanical stimuli (allodynia) and weight-bearing deficits. As assessed by MRI, we found a negative correlation between tumor volume and allodynia or postural deficits throughout the experiment. Using μCT, we found that the bone volume/total volume (BV/TV) ratios for trabecular and cortical bone correlated with both mechanical hypersensitivity and weight-bearing impairment. However, whereas trabecular BV/TV stabilized between days 7 and 10 post-tumor detection, the cortical bone loss reached its maximum at that time. Our imaging approach also allowed us to consistently detect the tumor before the onset of pain, paving the way for the preemptive identification of at-risk patients. Altogether, these results improve our understanding of the events leading to tumor-induced bone pain and could eventually help in the design of novel strategies for the management of bone diseases.

Keywords Metastasis · MRI · Micro-CT · Dynamic weight bearing · Allodynia

Introduction

Bone is the most common site of distant metastases in breast cancer [1]. At post-mortem examination, up to 70 % of all patients who die of breast cancer show bone lesions [2, 3]. In the United States alone, this percentage represents more than 150,000 patients among those experiencing invasive breast cancer [4]. Bone metastases in breast cancer patients most frequently induce osteolytic lesions, which increase the risk for skeletal-related events, such as pathological fractures and debilitating bone pain [5–7]. These skeletal complications are recognized to increase mortality, decrease the quality of life (through weight-bearing deficits and social isolation), and affect treatment strategies [8]. In particular, a recent review estimated that 65 % of bone metastasis patients were coping with pain, and one-third of

L. Doré-Savard · N. Beaudet · P. Sarret (✉)
Department of Physiology and Biophysics, Faculty of Medicine and Health Sciences, Université de Sherbrooke, 3001, 12e Avenue Nord, Sherbrooke, QC J1H 5N4, Canada
e-mail: philippe.sarret@usherbrooke.ca

L. Tremblay · M. Lepage
Department of Nuclear Medicine and Radiobiology, Faculty of Medicine and Health Sciences, Université de Sherbrooke, 3001, 12e Avenue Nord, Sherbrooke, QC J1H 5N4, Canada

Y. Xiao
The Center for Bone and Periodontal Research, McGill University, 740 Dr Penfield Avenue, Rm 2200, Montreal, QC H3A 1A4, Canada

these patients graded their pain as moderate to severe [9]. Further clinical investigations concluded that at least 45 % of cancer patients found their pain to be undermanaged [10, 11]. Bone cancer pain management thus remains challenging for researchers and clinicians.

The development of clinical applications has most likely been impeded in part by a lack of knowledge about the underlying mechanisms driving this chronic pain condition. In recent years, however, the establishment of preclinical animal models of metastasis-induced pain has significantly improved our understanding of the pathophysiology of bone cancer pain and has helped identify new molecular targets [12, 13]. In particular, the development of rodent animal models of bone cancer pain, based on the implantation of cancer cells into the medullary cavity of the long bones, has provided us with new insights on the mechanisms leading to bone cancer pain [14–17]. For instance, three main components of bone metastasis have been defined as pain-inducing factors: (1) nerve injury and sprouting caused by tumor growth [18–21], (2) inflammatory cascades and acidosis triggered by tumor and bone-associated cells [22–24] and (3) bone remodeling [25–27]. These animal models thus offer new opportunities for evaluating potential analgesic therapies to relieve bone cancer pain [28].

The detection and localization of metastatic bone lesions are important for determining the stage of breast cancer. Therefore, the use of powerful imaging technologies has become critical for the in vivo monitoring of tumor progression, assessment of bone integrity and measurement of therapeutic efficacy. Among the different bone imaging modalities, whole body scintigraphy, plain film radiography and computed tomography (CT) are often used to diagnose breast cancer bone metastases [29, 30]. However, single photon emission CT (SPECT or SPECT/CT), positron emission tomography (PET or PET/CT) and magnetic resonance imaging (MRI) are increasingly recommended to optimize the bone or tumor anatomical visualization and detect changes in tumor or bone metabolism [31–36].

The early diagnosis of bone metastasis may improve the patient's prognosis and quality of life [37–39]. Because bone pain is the most common symptom in breast cancer patients, relating it quantitatively to tumor growth and bone damage would enable all dimensions of cancer management to be improved. According to the most recent version of the response evaluation criteria in solid tumors [40], defining the osteolytic lesion size by CT and the soft-tissue impairment by MRI are the current standards for breast cancer patients with metastases [35]. In the present study, we therefore investigated whether bone cancer pain could be directly correlated with tumor progression and bone remodeling. We used an experimental model in which MRMT-1 mammary carcinoma cells were implanted in the medullary cavity of the femur of Sprague-Dawley rats [41]. We examined whether these two imaging modalities allowed an early, quantitative and temporal correlation with changes in the reflexive withdrawal responses to mechanical stimuli and the observation of weight-bearing deficits.

Materials and methods

Cell culture

Mammary rat metastasis tumor (MRMT-1) cells (carcinoma) were kindly provided by the Cell Resource Center for Biomedical Research Institute of Development, Aging and Cancer (Tohoku University 4-1, Seiryo, Aoba-ku, Sendai, Japan) and harvested in RPMI 1640 medium (Gibco, Montreal, QC, Canada) supplemented with 10 % fetal bovine serum (heat-inactivated) and 2 % penicillin/streptomycin (Gibco). The cells were detached by a brief exposure to 0.25 % w/v trypsin–EDTA (Gibco, Montreal, QC, Canada) and then prepared for femoral inoculation. Briefly, the cells were pelleted by centrifugation (3 min at $350\times g$), rinsed with 1 mL of Hank's balanced salt solution without calcium, magnesium or phenol (HBSS; Gibco, Montreal, QC, Canada) and further centrifuged using the same conditions. The pellet was re-suspended in 1 mL of HBSS, and the cells were counted with a hemocytometer. The cells were diluted to achieve a final concentration of 30,000 cells in 20 µL and maintained on ice prior to surgery.

Animals

Adult male Sprague-Dawley rats (200–225 g; Charles River Laboratories, St.-Constant, QC, Canada) were maintained on a 12 h light/dark cycle with access to food and water ad libitum. Animal-related procedures were approved by the Ethical Committee for Animal Care and Experimentation of the Université de Sherbrooke and conducted according to the regulations of the Canadian Council on Animal Care (CCAC). The rats were acclimatized to the animal facility for 4 days and to the manipulations and devices prior to the behavioral studies for 2 days. Note that the animals tested for pain and used for the imaging studies were the same except when several imaging procedures were performed on the same animals over time (Fig. 2). Indeed, multiple prolonged exposures to anesthesia tend to modify behavioral responses to pain.

Surgical induction of bone cancer

The surgical procedure was the same as in Doré-Savard et al. [41]. Briefly, the rats were laid supine, and the skin overlying the *quadriceps femoris* of the hind paw was shaved and disinfected with 70 % v/v ethanol. A minimal

skin incision (8–10 mm) exposed the *quadriceps femoris*. The *vastus lateralis* was incised (5–8 mm in length) to expose the femoral epicondyle while the patellar ligament remained untouched. The damage to the surrounding muscle and blood vessels was minimal. Using a 0.8 A stereotaxic drill (Foredom, Bethel, CT, USA) connected to a 1.75 mm carbide steel burr (Stoelting Co., WoodDale, IL, USA), a small and superficial cavity was burred between the medial epicondyl and the adductor tubercle (approximately 1 mm in depth). A 25-gauge needle was inserted into the cavity at a 45° angle, allowing it to reach the intramedullary canal of the femur. The needle was substituted with a blunt end 25-gauge needle connected to a 50 µL Hamilton syringe containing 20 µL of the MRMT-1 cancer cell suspension. The syringe was left in place for 1 min to allow cell dispersion within the bone marrow. The needle was then removed, and the cavity was sealed with dental amalgam (Prodigy A3, Kerr, Orange, CA, USA) that was polymerized with a curing light (QHL75, Dentsply, Milford, DE, USA). The site was thoroughly washed with sterile deionized water. The muscle, conjunctive tissue and skin were closed with sutures and washed with 3 % v/v hydrogen peroxide. The sham animals received the complete surgical procedure except for the implantation of mammary cells, which was replaced by vehicle injection (20 µL HBSS). The rats were housed individually for 24 h to allow recovery. As demonstrated previously [41], the impact of surgery was minimized by implantation at this anatomical site, which reduces the chances of patellar ligament or joint damage.

Behavioral analyses

The animals were tested on days 0, 7, 11, 14, 18 and 21 after cell implantation. For von Frey testing, the rats were placed in enclosures on an elevated wire mesh floor, and mechanical allodynia was assessed using a dynamic plantar aesthesiometer (Ugo Basile, Stoelting, IL, USA). A metal probe (0.5 mm diameter) was directed against the hind paw pad, and an upward force was exerted (3.33 g/s). The force required to elicit a withdrawal response was measured in grams and automatically registered when the paw was withdrawn or the preset cut-off was reached (50 g). Five values were taken alternately on both the ipsilateral (operated side) and contralateral hind paws at intervals of 15 s. The rats were acclimatized to the enclosures for 2 days prior to testing.

The dynamic weight bearing (DWB) assessment was performed according to the procedure described by Tétreault et al. [42]. In brief, the DWB device (Bioseb, Boulogne, France) consisted of a Plexiglas enclosure (22 × 22 × 30 cm) with a floor sensor composed of 44 × 44 captors (10.89 mm^2 per captor). A digital camera was placed beside the cage and was pointed towards the enclosure. The rats were allowed to move freely within the apparatus for 5 min while the pressure data and live recording were transmitted to a laptop computer via a USB interface. The raw pressure and visual data were colligated with the DWB software v1.3 (Bioseb). A zone was considered valid when the following parameters were detected: ≥4 g on 1 captor with a minimum of 2 adjacent captors recording ≥1 g. For each time segment in which the weight distribution was stable for more than 0.5 s, the zones that met the minimal criteria were then validated and assigned as either right or left hind paw or front paw by an observer according to the video and the scaled map of the activated captors. Finally, a mean value for the weight on every limb was calculated for the whole testing period based on the length of time of each validated segment. The animals were not acclimatized to the enclosure before the initial testing period to maximize the exploration behaviors. For the behavioral analyses shown in Fig. 1, the time axis was based on the post-implantation days, ranging from 0 to 21.

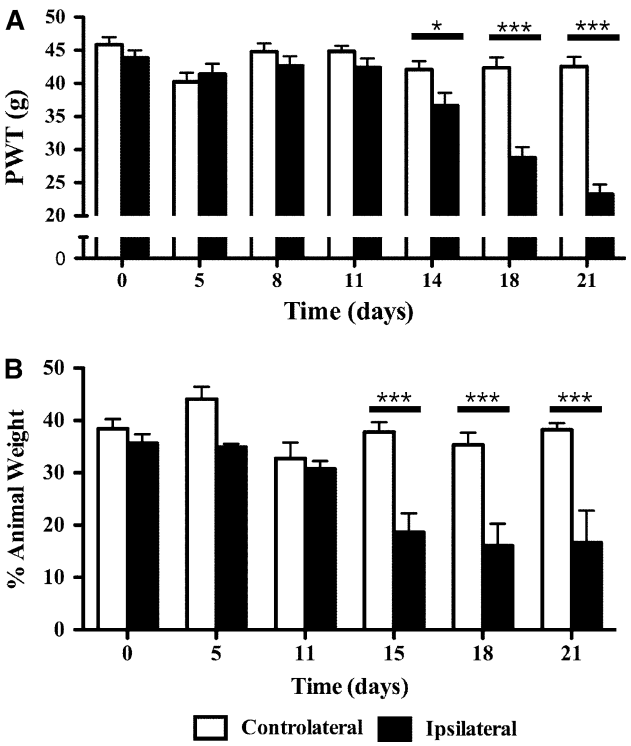

Fig. 1 Behavioral evaluation of bone cancer pain over time. **a** Allodynia is determined using the von Frey test following tumor implantation. In cancer-bearing rats, the PWT decreases progressively from days 11–14 in response to innocuous stimulations ($n = 10$). **b** Quantification of DWB in the implanted animals, expressed as the percentage of animal weight ($n = 7$). A significant difference in the weight distribution on the ipsilateral paw is observable from day 15 until reaching its maximum level at day 21, with a decrease of 56 % in the weight borne. The contralateral paw remains unaffected throughout the behavioral testing. The *asterisks* denote a significant difference from the contralateral paw; * $p < 0.05$; *** $p < 0.001$

MRI

MRI studies were conducted at the Centre d'imagerie moléculaire de Sherbrooke (CIMS) with a 210 mm small-animal 7T scanner (Agilent Technologies Inc., Palo Alto, CA, USA) and a 63 mm volume RF coil. The rats were placed in the supine position in an MRI compatible cradle equipped with a custom-made paw support designed to position both limbs stably and reproducibly. The animals were anaesthetized with 3 % (induction) and 1.5 % (stabilization) isoflurane in oxygen. A feedback-controlled animal warm-air heater system was used to keep the animal's body temperature at physiological levels, and the respiration rate was continuously monitored (SA Instruments Inc., Stony Brook, NY, USA). The MRI protocol included the acquisition of axial (sagittal) pre-contrast and 10 min post-contrast T1-weighted images using a gradient echo sequence with TR of 210 ms, TE of 3.35 ms, flip angle of 30°, matrix of 256 × 256, FOV of 60 × 60 mm^2, NA of 8 (30 sagittal slices), and thickness of 1.5 mm. A 500 mL bolus of the contrast agent (Gd-DPTA, Magnevist, Berlex) was injected via the tail vein. The animals were imaged 9, 11, 13, 15, 18 and 21 days after the tumor implantation. To evaluate the tumor invasiveness, a region of interest (ROI), including the whole bone cortex, medullary channel of the femur and emerging tumor outside the bone when present, was defined for each slice displaying bone or tumor tissue. This ROI yielded a voxel intensity histogram for both hind paws. The contralateral maximal voxel intensities were used to set the pathological threshold. Every ipsilateral voxel remaining was colored according to its intensity on a yellow–red scale. The data analysis and calculations were programmed in the Matlab environment (Version 7.10; MathWorks Inc., Natick, MA, USA).

μCT

The μCT scans were performed using a high resolution Micro-CT (μCT) scanner (SkyScan-1072, Aartselaar, Belgium), and the subsequent 3D architecture analyses were completed using the associated software applications. The scanner was equipped with a sealed microfocus X-ray tube with a power source ranging from 20 to 100 kV (0–250 μA) and an X-ray CCD-camera based on a cooled 12-bit CCD-sensor of 1,024 × 1,024 pixels.

In the present study, the distal femurs, wrapped with parafilm to prevent dehydration, were scanned at a source power of 80 kV/124 μA and a spatial resolution of 14.06 μm/pixel. The rotation was set at 0.9°/step for 180°, and the exposure time was set at 3.0 s/step. The reconstruction of the dataset of the X-ray shadow images obtained from the scans was performed using NRecon (version 1.6.1.3), generating a dataset of cross-sections that was then used for the analysis of the 3D architectural parameters and the creation of 3D models with CT-Analyzer (version 1.10.01). The ratios of bone volume over total volume (BV/TV) for the trabecular and cortical bones were determined by defining the volumes of interest (VOI) over a range of 5.63 mm starting from the growth plate. For the imaging analysis shown in Figs. 2 and 4, the time axis was based on the post-detection days, ranging from 1 to 10, with day 1 being the time of the first detection of a bone tumor by MRI. This normalization was performed to reduce the inter-individual variations.

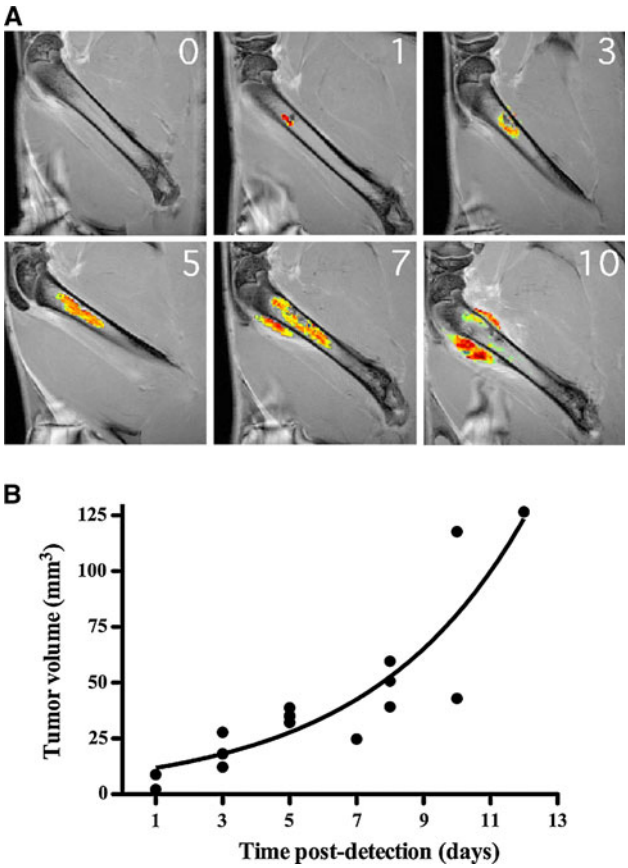

Fig. 2 Estimation of tumor volume using contrast-enhanced (Gd-DTPA) MRI. **a** Enhanced contrast is observed from day 1 (post-detection) in a small area adjacent to the injection site. The tumor size then progresses and invades the distal medullar channel without altering the cortical integrity (days 3 and 5). At a later stage, the tumor emerges from the bone, expanding mainly outside the bone between the cortical line and periosteal membrane. Meanwhile, the contrast intensity is decreased in the medullar channel as the necrosis spreads throughout the channel. In addition, the cortical line is blurred in thinner regions. **b** Each animal in which a tumor is detected is monitored at several time points and reported with respect to post-detection time to reduce the variability. The tendency curve shows the exponential growth pattern

Statistical analyses

The von Frey and dynamic weight-bearing data were analyzed using a two-way ANOVA followed by Bonferroni's post hoc test. The Spearman non-parametric correlation test was used to compare the behavioral, MRI and μCT data because normality could not be assumed (failed KS test with Dallal–Wilkinson–Lillie for the p value and visual histogram distributions). Linear and non-linear regressions were displayed on graphs as guides to the eye. The non-linear model used for Figs. 3 and 6 was either a one- or two-phase decay described by the following equation (provided by Graphpad Prism 5.0 software): Y = Plateau + Spanfast*exp(-KFast*X) + Spanslow*exp (-KSlow*X), where KFast and KSlow (K for a one-phase decay) are the rate constants describing the speed at which the dependent variable is decreasing.

Results

Temporal development of behavioral nociceptive responses following the implantation of breast carcinoma cells in the femur

We monitored the onset of pain and its evolution on a regular basis during the first 3 weeks following the inoculation of the syngeneic mammary tumor cell line MRMT-1 into the femoral bone. We first assessed tactile allodynia using the von Frey test (Fig. 1a). Mechanical hypersensitivity was demonstrated on day 14 post-surgery by a reduced paw withdrawal threshold (PWT) compared with the contralateral hind paw (36.7 ± 2.0 vs. 42.1 ± 1.3 g, respectively; $p \leq 0.05$). Allodynia progressively developed until day 21, reaching a 45 % decrease of the mechano-nociceptive threshold (23.3 ± 1.4 vs. 42.6 ± 1.5 g; $p \leq 0.001$). Tumor-bearing rats displayed no change in their withdrawal thresholds on their contralateral hind paw (Fig. 1a).

The measurement of the weight-bearing deficits in freely moving rats has recently been proposed as a potential endpoint to the quality of life assessment [42]. Therefore, we evaluated the effects of tumor-induced bone remodeling on the changes in weight bearing using DWB technology (Fig. 1b). Our results revealed that the weight borne by the tumor-implanted limb had decreased significantly at day 15 (18.6 ± 3.6 %) when compared with the weight borne at day 11 (30.7 ± 1.5 %) (Fig. 1b). The maximal alteration of the weight distribution was reached 21 days following the cancer cell inoculation (38.2 ± 1.3 % on the contralateral paw vs. 16.6 ± 6.1 % on the ipsilateral paw; $p \leq 0.001$). Note that the rats transferred their ipsilateral hind paw weight mainly to the forepaws and consequently

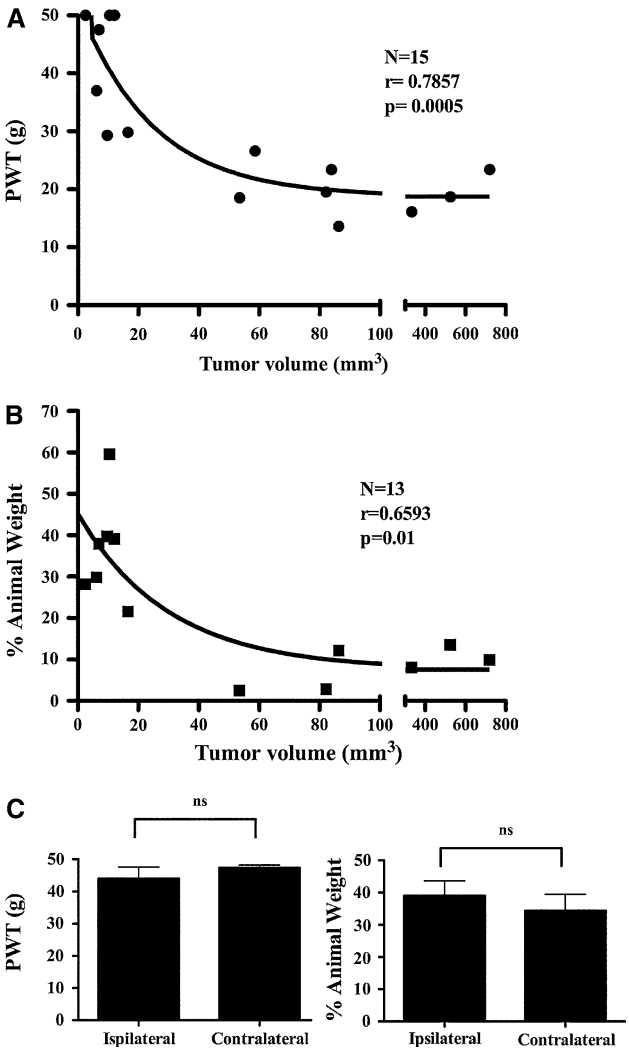

Fig. 3 Correlation between the tumor volume and behavioral measurements of bone cancer pain. **a** The estimated tumor volume is inversely correlated with the PWT. **b** The same pattern is observed when the volume is correlated with the percentage of animal weight borne by the affected paw. Both parameters stabilize at high tumor volumes. **c** The comparison between the ipsilateral and contralateral paws of the cancer-bearing animals shows no significant difference at day 1 post-detection, confirming the assumption that the tumor was detected using MRI before the onset of pain

decreased their exploratory behaviors, grooming and rearing (data not shown). No significant difference was noted for the 21-day period between the sham animals and the contralateral hind paw of the cancer rats.

Tumor growth monitoring using MRI

We first monitored the tumor progression by scanning the rats at short intervals to capture the tumor growth in the femur at early stages of development. The volume of the detected tumor was analyzed as a function of the post-detection time to normalize the inter-individual variability

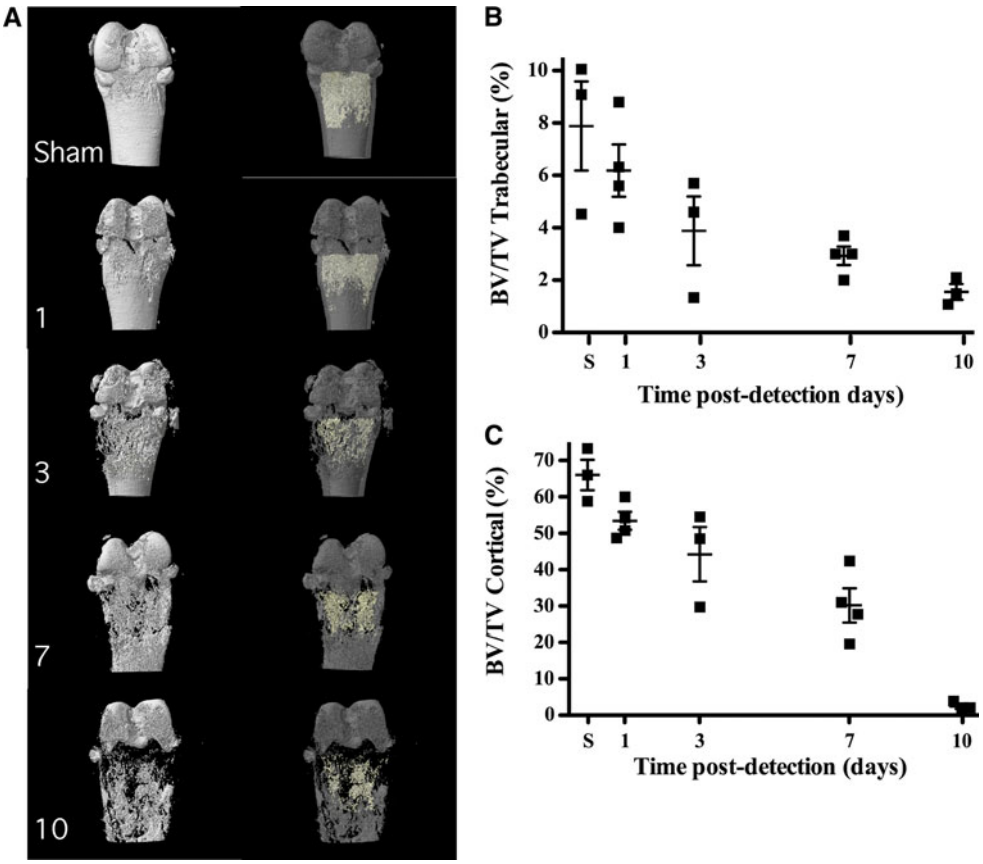

Fig. 4 μCT analysis of sham and tumor-bearing rat femurs. **a** Typical reconstruction of the sham-operated femur and cancer-bearing bones at days 1, 3, 7 and 10 post-detection. A well-organized trabecular structure and smooth cortical surface are observed on the sham-operated bone. Conversely, the trabecular is slightly degraded at day 1 of tumor development (post-detection), whereas the cortex remains unaffected at that stage. However, the cortical bone is partially resorbed and the trabecular architecture is clearly lost at days 3 and 7. At day 10, the tumor has resorbed most of the cortical bone and has expanded beyond the bone compartment. **b**, **c** The BV/TV ratios for the trabecular and cortical bone decrease over time. The trabecular BV/TV tends to stabilize between days 7 and 10 post-detection, whereas the cortical degradation is maximal during this period

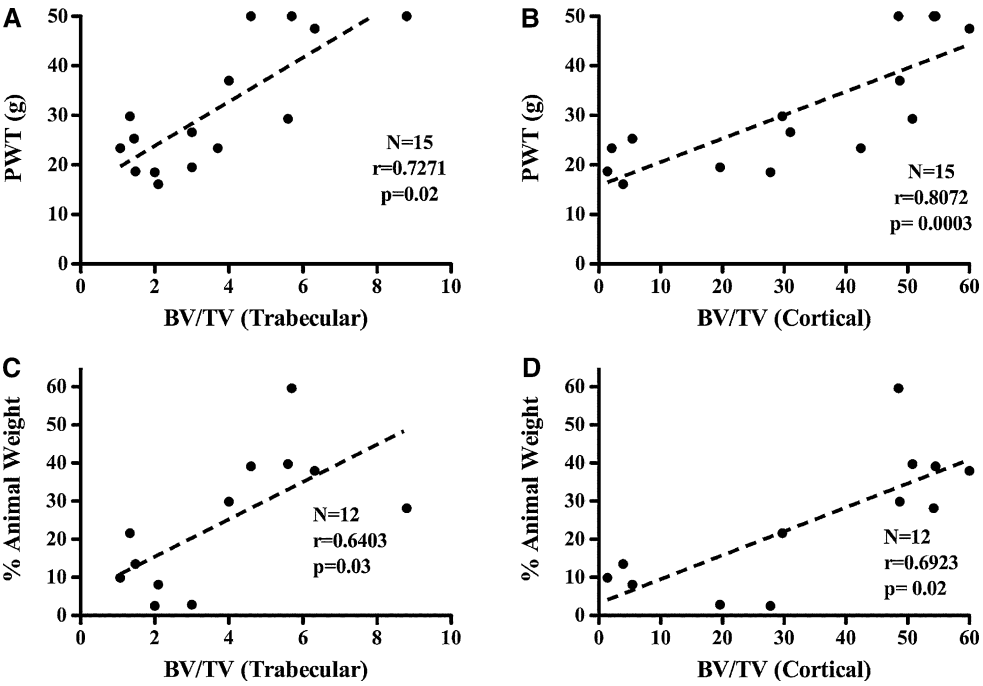

Fig. 5 Correlation between bone resorption and pain-related behaviors. **a**–**b** A positive correlation is observed between the trabecular or cortical BV/TV ratios and PWT. **c**, **d** A significant correlation is also observed when comparing the trabecular or cortical BV/TV with the % of animal weight borne by the tumor-bearing paw

in tumor development. For example, the sensitivity of the sagittal gadolinium-enhanced T_1-weighted MRI allowed us to detect intra-osseous tumors smaller than 10 mm^3 in some cancer-bearing rats. These small foci were considered to be day 1 post-detection and corresponded to days 8–10 post-implantation of MRMT-1 cancer cells. The bone

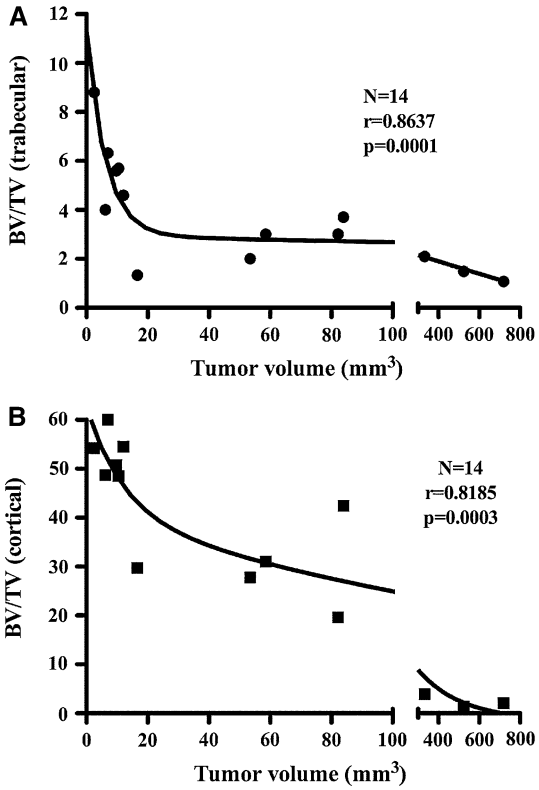

Fig. 6 Correlation between the estimated tumor volume and bone remodeling. **a** The tumor volume is significantly correlated with the trabecular BV/TV. This parameter decreases drastically at volumes smaller than 20 mm^3. **b** In cancerous bones, the tumor volume is correlated with the cortical BV/TV with decreasing BV/TV throughout the tumor development

tumor development and structural damages to the femur were further monitored for up to 10 days post-detection (Fig. 2a). At day 0, the MR images of the marrow and trabecular bone all displayed uniform signal intensities. The sharp but hypointense cortical line was continuous. At day 1 post-detection, the MRI revealed an increased signal intensity in the area immediately surrounding the injection site, thereby revealing the success of the tumor implantation and growth in the medullary cavity. During days 3–5, the carcinoma spread into the medullary canal, progressively reaching the distal metaphysis to the implantation site. At this stage, the tumor volumes ranged from 30–40 mm^3 (Fig. 2b). On day 7 post-detection, a hyperintense signal in the diaphyseal bone revealed deep infiltration. Furthermore, the contrast-enhanced T_1-weighted images revealed the presence of periosseous tumor extension across the irregular and blurred cortical bone line near the distal metaphysis. Note that after dissection, we noticed that the tumor remained confined to the periosteal compartment (data not shown). This mechanical distension and stretching of the periosteum is known to contribute to the development of pain [19, 43]. As previously described [41], the hypointense signal detected at day 10 post-detection in the medullary cavity is the consequence of the presence of necrotic cells. The first half of the growth curve shows a linear progression of the carcinoma, consecutive to the implantation and setting of the cells in their new environment ($n = 19$; Fig. 2b). Then, the curve takes an exponential profile from day 8, which is the stage where the periosseous signal is captioned.

Correlation between tumor growth and pain-related behaviors

We verified the potential relationship between tumor size and pain-related behavioral modifications by performing the von Frey and DWB tests before the acquisition of the T_1-weighted contrast enhanced MR images (Fig. 3). We observed a strong negative correlation between tumor volume and the mechanical threshold (Fig. 3a) throughout the experiment ($r = 0.7857$; $p = 0.0005$). The evolution of these parameters displayed a two-phase decay in which the allodynia was maximal at volumes >80 mm^3. The rate constant (k) of $1.34E10^6$ (fast) confirms the fast onset of allodynia at an early stage. The rate stabilizes ($k = 0.04$) at approximately 10 % of the maximal size the tumor will reach. Similarly, a moderate correlation was revealed between the tumor volume and weight bearing ($r = 0.6593$; $p = 0.01$) (Fig. 3b). This time, the variation was extrapolated in a one-phase decay model with a slower rate constant ($k = 0.03$). The results suggest that the early onset of pain is an indicator of tumor progression. To verify this observation, we examined whether allodynia and postural impairment could be markers of tumor development at an initial stage (Fig. 3c). For a tumor of <10 mm^3 corresponding to day 1 post-detection, no behavioral difference between the ipsi- and contralateral paws was observed. We thus concluded that imaging can systematically reveal the presence of a tumor before the onset of pain in our model.

Bone resorption monitoring with μCT

Advanced breast cancer commonly disseminates and leads to osteolytic bone metastases [1]. To further quantify the structural changes of the affected bones, we therefore performed post-mortem μCT analyses at four time points (days 1, 3, 7 and 10 post-detection) after cancer cell injection and in the sham animals ($n = 3$–4). The bone samples were collected from the animals previously imaged in the MRI (c.f. Fig. 3). The reconstructed 3-D μCT images of the carcinoma-implanted femurs showed the progressive tumor-induced osteolysis (Fig. 4a). In contrast to the intact bone architecture of the sham animals, the cancer-bearing rats exhibited severe bone lesions, as

represented by the decrease in the trabecular and cortical morphometric parameters (Fig. 4b, c). At day 1 post-detection, the trabecular modifications already occurred, while the bone cortex remained mainly unaffected. Indeed, the trabecular BV/tissue volume ratio progressively decreased by 70 % between days 1 and 10 (Fig. 4b). The same trend was observed for the cortical bone, with the BV/TV decreasing significantly by more than 95 % on day 10 compared with day 1 (Fig. 4c). However, cortical degradation was only detected on day 7. At that stage, cell leakage through the cortex is possible because massive osteopenia was revealed in several areas of the metaphysis. Accordingly, tumor growth outside the cortex was monitored in the MRI on days 7–10 post-detection. Thus, the trabecular and cortical bone degradation profiles are different at a late stage. Indeed, the trabecular BV/TV stabilizes between days 7 and 10 (with only an 8.8 % decrease), whereas the cortical bone loss is maximal during the same period. Nearly 90 % of the remaining bone cortex on day 7 was resorbed before the last experimental day (day 10). Significant differences were observed at days 7 and 10 post-detection at the trabecular level compared with the sham animals and at day 10 at the cortical level ($p \leq 0.05$).

Correlation between bone resorption and tumor-induced pain

We further examined whether the behavioral deficits were correlated with bone architecture alterations. In the animals used for the behavioral and imaging experiments, a strong positive correlation was shown between the trabecular bone content and mechanical threshold (Fig. 5a; $r_s = 0.73$; $p = 0.002$). The Spearman correlation was stronger against the cortical bone content alteration (Fig. 5b; $r_s = 0.81$; $p = 0.0003$), suggesting that these parameters could be used as potential markers for the clinic. However, the correlations appeared to be moderate in terms of a weight-bearing deficit either when verifying against the trabecular content (Fig. 5c; $r_s = 0.64$; $p = 0.03$) or the cortical content (Fig. 5d; $r_s = 0.69$; $p = 0.02$). Overall, the trend in the data suggests that a one percent decrease in the trabecular BV/TV ratio results in a drop of 4.5 ± 1.0 g in the PWT and 4.9 ± 1.7 % in the ipsilateral paw load. Conversely, a decrease of one percent in the cortical BV/TV is less aggressive on the behavioral variables, reflected in variations of 0.5 ± 0.1 g (PWT) and 0.6 ± 0.2 %, respectively.

Correlation between tumor volume and bone resorption

Next, we verified the correlation between the growth of the tumor and the extent of the BV/TV ratio decrease (Fig. 6). We found a strong negative correlation against both the trabecular (Fig. 6a; $r_s = 0.82$; $p = 0.0003$) and cortical (Fig. 6b; $r_s = 0.86$; $p = 0.0001$) bone content. The decay curve shows that the trabecular BV was affected at an early stage of tumor development and remained at a low level thereafter. The cortical bone BV/TV ratio, however, decreased more in proportion to the tumor growth. Indeed, the decay rate constants were 133 times higher for the trabecular content than for the cortical content. These results were in line with the observations made in the MRI, in which the tumor growth spread first in the medullary canal, replacing the marrow and trabecular bone while progressively degrading the compact cortex for an ultimate periosteal expansion at a late stage.

Discussion

Bone metastases lead to a painful condition for which available treatments have limited efficacy. Opioids have remained the gold standard for advanced cancer pain management for the last 25 years, despite their many undesirable effects [44]. For example, morphine has been associated with opioid-induced hyperalgesia, tolerance and constipation [45]. Additionally, King and colleagues reported deleterious effects of morphine on bone integrity in a mouse cancer model [46]. This effect appeared to be mediated through the activation of osteoblasts, increasing the risk of bone fractures. It has become clear that new treatments are needed to improve cancer patients' quality of life, especially given recent increases in post-diagnosis life expectancy [4]. Additionally, scientists and clinicians are highly receptive to new tools or methodologies to improve the monitoring of not only the analgesic effects of treatments but also other related parameters, such as tumor growth and bone remodeling [28, 38, 39]. In that respect, the use of advanced non-invasive imaging modalities appears to be a good solution to visualize various aspects of the bone environment in terms of soft-tissue content, density, or metabolism [29, 30]. The aim of this study was thus to evaluate the correlation between MRI or μCT imaging and pain-related behaviors in an animal model of bone cancer.

Previous population-based cohort studies have highlighted the high incidence of skeletal-related events among breast cancer patients with bone metastases following the first year of a bone metastasis diagnosis [8]. Therefore, diagnostic imaging modalities are important because the early identification of bone metastases could lead to changes in patient management and quality of life. Among the technologies used to image bone tumors, MRI seems to yield a reliable diagnostic outcome in terms of sensitivity and specificity [35, 47]. Indeed, the high soft tissue resolution of MRI provides detailed images of bone tumors and

bone marrow lesions. In addition to clinical practice, MRI has also been used for the early detection of bone metastases in animal models [48, 49]. Furthermore, MRI appears to be efficient for monitoring tumor progression in correlation with histological and biochemical parameters, such as osteoclastic activity or serum-specific antigen levels [50, 51]. More recently, the evaluation of different treatments targeting bone tumors has been performed with imaging techniques, such as diffusion weighted- and dynamic contrast-enhanced MRI [35, 52, 53].

Although bone remodeling and pain appear to be intimately linked, the relationship between tumor growth-induced bone resorption and pain-like behaviors has been poorly investigated. Although it is most commonly detected in advanced stages, patients can often present with bone pain as the first symptom of cancer, particularly in breast cancer [11]. Therefore, establishing such a relationship would increase our comprehension of the effect of an anti-tumorigenic drug on both cancer- and pain-related events. For example, the selective COX-2 inhibitor, MF tricyclic, was shown to reduce tumor growth and bone damage in addition to inducing an analgesic effect [22]. A similar case was reported with zoledronate, a bisphosphonate tested in a rat cancer model [54]. However, for those drugs, the analgesic effect was determined at a late stage only, and the timely effect of the drug on both variables was not determined.

The model used in the present study mimics the development of a bone metastasis that could occur after the dissemination of tumor cells to the bone through blood circulation. However, the surgical procedure bypasses the extravasation of cancer cells from the primary organ to the bone. Models of the orthotopic implantation of cancer cells to a primary site or systemic dissemination through intravenous or intracardiac administration have also been used in the past to mimic the holistic context of metastatic cancer. Although these models have been very helpful in elucidating the underlying mechanism involved in metastatic processes, they are of limited usefulness for specific pain investigations. Indeed, pain evaluation in rodents is mostly based on the differences between an injured paw and its healthy counterpart. Evaluating pain in an animal with numerous bone lesions would thus be problematic, particularly with the potential colonization of peripheral organs and tissues. That being said, more common cell types have been used in several contexts, which allows for a comparison of the bone lesions induced. As an example, human MDA-MB-231 mammary cells that are injected intracardially induce bilateral long bone metastasis 30–55 days after inoculation [55, 56]. The radiological and histological aspects of these tumors appeared to be very similar to those from bone-inoculated cells [19, 33]. From the moment of the detection of bone tumors (28 days in the case of MDA-MB-231 cells directly administered into the bone), the time course of tumor development was also very similar. We are thus confident that our model of tumor implantation in the bone, without the holistic metastatic context, is still relevant and allows for the efficient study of bone metastasis-induced pain. Additionally, the timeline with which the tumor grows is dependent on the chosen implantation site and the number of cells injected. However, with MRMT-1 and NCTC2472 cells, the injection of a higher number of cells has been demonstrated to trigger pain at an earlier stage without significantly modifying the severity or rapidity of the evolution of the symptoms in the animals [14, 16, 57].

In the present study, our MRI results show moderate to strong correlations and a two-phase profile between pain and cancer growth. Indeed, the variation in pain is greater at an early stage of tumor growth but tends to stabilize thereafter. This trend may be attributable to an early modification in the bone innervation and vasculature. The MRI shows the initial infiltration of the medullary canal, affecting the red marrow. This two-phase profile is also supported by our μCT data, which revealed a rapid drop in the BV/TV trabecular ratio at the same time. Meanwhile, a progressive degradation of the cortical bone slowly creates an access to the cortex and periosteal compartment. Recently, nerve sprouting was shown to be associated with cancer pain, especially at the periosteal level [19, 20, 58, 59]. Nerve sprouting occurs when the bone integrity is compromised and when the cancer cells act directly on the periosteal membrane [18, 60]. On the other hand, advanced tumor growth was shown to induce nerve endings injury resulting in a decrease in CGRP/NF200-positive innervation in bone marrow and cortex [60]. Nerve injury induced the expression of several markers of central sensitization including neuronal damage marker ATF-3 [41, 61, 62]. Both sensory and sympathetic fibers are implicated and the proliferation of nerve endings has been compared to neuroma, and involved in pain [59, 63]. MR images showed enhanced contrast at the bone periphery as early as day 5 post-detection. Therefore, the occurrence of a striking onset of mechanical hypersensitivity at early tumor development is not surprising. After this early pain onset, allodynia progressed slowly, even if the tumor dimension expanded from 60 to more than 700 mm^3. This finding supports the hypothesis that the bone microenvironment is central to the genesis of tumor-induced pain. This observation also raises the possibility that growth in the periosseous tissues is not a major factor in ongoing pain. However, we hypothesize that the distension of the periosteal compartment could be responsible for spontaneous pain events at the late stages. Nevertheless, the evaluation of the role of periosseous tissue compared to bone remains a challenge to evaluate in pre-clinical settings. The other

question that remains is whether a reduction in tumor size would result in less pain. Radiotherapy has been associated with pain relief in animal models [64]. We believe this outcome should be evaluated in the future with a protocol such as the one we are proposing here.

Metastatic breast cancer in bones also leads to other severe pain events, such as the fracture of a weight-bearing limb. Indeed, lytic lesions can result in a 60–90 % reduction in bone strength, which increases the risk of pathological fractures [65]. Early symptoms of pain or functional compromise can thus reveal an impending emergency, requiring proactive therapeutic intervention. Determining the extent of the osteolytic lesions by μCT therefore represents a useful approach to detect any structural defects in the cortical and trabecular content or to visualize bone marrow metastases [47]. The morphological analyses of the femoral bone by μCT revealed significant linear correlations between the BV/TV ratios at the cortical or trabecular levels and touch-evoked pain or weight-bearing deficits. These results are supported by a previous study demonstrating a link between tumor growth-induced bone destruction and behavioral pain manifestations [66].

It is now established that bone remodeling provokes the release of cytokines and growth factors that stimulate nociceptors directly [13]. Additionally, the increased osteoclastic activity in the vast majority of bone metastases secondary to breast cancer creates an acidic microenvironment that activates transient receptor potential channels and acid-sensing ion channels, increasing nociceptive firing [24, 67, 68]. Furthermore, nerve endings in the bone cortex become exposed to factors released by the tumor and the bone matrix after resorption. Marketed drugs counteracting the osteolytic hyperactivity, such as bisphosphonates and RANKL pathway inhibitors, proved useful in pre-clinical and clinical contexts for reducing the incidence of skeletal-related events and collagen blood levels and at increasing survival rates [69]. The effects of these drugs on pain-related behaviors are, however, rarely investigated. The progressive and timely decrease in the cortical/trabecular BV and relationship to pain make them relevant variables to investigate in drug screening. Therefore, anti-resorptive treatments would be expected to alleviate or reduce pain manifestations in an indirect way by slowing down bone remodeling. Accordingly, there is evidence that anti-resorptive drugs indirectly reduce pain through the inhibition of osteolysis [70, 71]. The nitrogen-containing bisphosphonate zoledronate, increasingly considered as an adjuvant in cancer therapy in addition to its anti-resorptive action [72], could fit the model we described here. Some cancer treatments cannot be excluded as having analgesic properties in addition to their primary antineoplastic action.

Our approach will also be improved in the future with PET experiments using a sodium fluoride tracer to assess bone metabolism at the time of the behavioral testing. Other bone-specific tracers are being developed to monitor the metabolism in bone resorption. Anderson et al. recently published a study on the use of an $\alpha v\beta_3$-targeted radiolabeled tracer that allows the accurate assessment of the relative number of osteoclasts in vivo [73]. Such a highly specific approach could easily be translated to bone cancer pain because osteoclast proliferation and activation are major factors in the development and maintenance of bone pain.

Conclusion

The continued medical care of patients who experience skeletal-related events represents an important health care cost that requires prevention strategies. Indeed, a one-year study of the incidence of skeletal-related events revealed that half of the patients with bone metastases each cost an average of $12,500 for only one event [74]. Therefore, the strong correlation between pain-related behaviors, tumor progression and bone remodeling revealed here suggests that pain and weight-bearing deficits are important indicators of the presence of bone metastases. Thus, patients reporting a change in pain intensity would need to undergo a closer examination to evaluate the disease progression. Additionally, MRI and μCT imaging modalities could accurately predict disease progression and be beneficial for monitoring the response to antitumor therapy or analgesic treatments. Finally, the fact that the pain-related behaviors are systematically detected after the appearance of the tumor in our protocol raises interest in a prophylactic analgesic treatment to prevent bone cancer pain onset. These elements are all expected to improve the quality of life for patients dealing with advanced stage cancer.

Acknowledgments This work is supported by grants from the Canadian Institutes of Health Research (CIHR) and the Cancer Research Society (CRS) awarded to P.S. It was also initiated by financial support from the Quebec Bio-Imaging Network and the network for Oral and Bone Health Research. L.D.-S. is the recipient of a Frederick Banting and Charles Best CIHR scholarship and is a trainee supported by the Canadian Arthritis Network. M.L. is the Canadian Research Chair in MRI. P.S. is a CIHR new investigator and director of the Sherbrooke's Neuroscience Center. P.S. and M.L. are members of the FRSQ-funded Centre de recherche clinique Étienne-Lebel. We are also grateful to Nathalie Carrier at the Centre de Recherche Clinique Etienne-Lebel for her help with the statistical analysis.

References

1. Weilbaecher KN, Guise TA, McCauley LK (2011) Cancer to bone: a fatal attraction. Nat Rev Cancer 11(6):411–425
2. Coleman RE (2006) Clinical features of metastatic bone disease and risk of skeletal morbidity. Clin Cancer Res 12(20 Pt 2): 6243s–6249s

3. Suva LJ et al (2011) Bone metastasis: mechanisms and therapeutic opportunities. Nat Rev Endocrinol 7(4):208–218
4. Jemal A et al (2010) Cancer statistics, 2010. CA Cancer J Clin 60(5):277–300
5. Trinkaus M et al (2009) Examination of the mechanisms of osteolysis in patients with metastatic breast cancer. Oncol Rep 21(5):1153–1159
6. Rove KO, Crawford ED (2009) Metastatic cancer in solid tumors and clinical outcome: skeletal-related events. Oncology 23(14 Suppl 5):21–27
7. Coleman RE (1997) Skeletal complications of malignancy. Cancer 80(8 Suppl):1588–1594
8. Jensen AO et al (2011) Incidence of bone metastases and skeletal-related events in breast cancer patients: a population-based cohort study in Denmark. BMC Cancer 11:29
9. van den Beuken-van Everdingen MH et al (2007) Prevalence of pain in patients with cancer: a systematic review of the past 40 years. Ann Oncol 18(9):1437–1449
10. Kirou-Mauro AM et al (2009) Has pain management in cancer patients with bone metastases improved? A seven-year review at an outpatient palliative radiotherapy clinic. J Pain Symptom Manag 37(1):77–84
11. Paes FM et al (2011) Radiopharmaceuticals: when and how to use them to treat metastatic bone pain. J Support Oncol 9(6):197–205
12. Pacharinsak C, Beitz A (2008) Animal models of cancer pain. Comp Med 58(3):220–233
13. Jimenez-Andrade JM et al (2010) Bone cancer pain. Ann N Y Acad Sci 1198:173–181
14. Schwei MJ et al (1999) Neurochemical and cellular reorganization of the spinal cord in a murine model of bone cancer pain. J Neurosci 19(24):10886–10897
15. Mao-Ying QL et al (2006) A rat model of bone cancer pain induced by intra-tibia inoculation of Walker 256 mammary gland carcinoma cells. Biochem Biophys Res Commun 345(4): 1292–1298
16. Medhurst SJ et al (2002) A rat model of bone cancer pain. Pain 96(1–2):129–140
17. Zhang RX et al (2005) Spinal glial activation in a new rat model of bone cancer pain produced by prostate cancer cell inoculation of the tibia. Pain 118(1–2):125–136
18. Halvorson KG et al (2006) Similarities and differences in tumor growth, skeletal remodeling and pain in an osteolytic and osteoblastic model of bone cancer. Clin J Pain 22(7):587–600
19. Bloom AP et al (2011) Breast cancer-induced bone remodeling, skeletal pain, and sprouting of sensory nerve fibers. J Pain 12(6):698–711
20. Jimenez-Andrade JM et al (2010) Pathological sprouting of adult nociceptors in chronic prostate cancer-induced bone pain. J Neurosci 30(44):14649–14656
21. Jimenez-Andrade JM et al (2011) Preventive or late administration of anti-NGF therapy attenuates tumor-induced nerve sprouting, neuroma formation, and cancer pain. Pain 152(11): 2564–2574
22. Sabino MA et al (2002) Simultaneous reduction in cancer pain, bone destruction, and tumor growth by selective inhibition of cyclooxygenase-2. Cancer Res 62(24):7343–7349
23. Fox A et al (2004) Anti-hyperalgesic activity of the cox-2 inhibitor lumiracoxib in a model of bone cancer pain in the rat. Pain 107(1–2):33–40
24. Nagae M, Hiraga T, Yoneda T (2007) Acidic microenvironment created by osteoclasts causes bone pain associated with tumor colonization. J Bone Miner Metab 25(2):99–104
25. El Mouedden M, Meert TF (2007) The impact of the opioids fentanyl and morphine on nociception and bone destruction in a murine model of bone cancer pain. Pharmacol Biochem Behav 87(1):30–40
26. Sevcik MA et al (2004) Bone cancer pain: the effects of the bisphosphonate alendronate on pain, skeletal remodeling, tumor growth and tumor necrosis. Pain 111(1–2):169–180
27. Tripathy D, Body JJ, Bergstrom B (2004) Review of ibandronate in the treatment of metastatic bone disease: experience from phase III trials. Clin Ther 26(12):1947–1959
28. Jimenez Andrade JM, Mantyh P (2010) Cancer pain: from the development of mouse models to human clinical trials. Translational pain research: from mouse to man. Frontiers in Neuroscience. CRC Press, Boca Raton
29. Costelloe CM et al (2009) Imaging bone metastases in breast cancer: techniques and recommendations for diagnosis. Lancet Oncol 10(6):606–614
30. Houssami N, Costelloe CM (2012) Imaging bone metastases in breast cancer: evidence on comparative test accuracy. Ann Oncol 23(4):834–843
31. Hsu WK et al (2008) Characterization of osteolytic, osteoblastic, and mixed lesions in a prostate cancer mouse model using 18F-FDG and 18F-fluoride PET/CT. J Nucl Med 49(3):414–421
32. Zitzmann-Kolbe S et al (2010) D-18F-fluoromethyl tyrosine imaging of bone metastases in a mouse model. J Nucl Med 51(10):1632–1636
33. Cheng C et al (2011) Evaluation of treatment response of cilengitide in an experimental model of breast cancer bone metastasis using dynamic PET with 18F-FDG. Hell J Nucl Med 14(1):15–20
34. Merz M et al (2011) Sorafenib tosylate and paclitaxel induce antiangiogenic, anti-tumour and anti-resorptive effects in experimental breast cancer bone metastases. Eur J Cancer 47(2): 277–286
35. Bauerle T et al (2010) Drug-induced vessel remodeling in bone metastases as assessed by dynamic contrast enhanced magnetic resonance imaging and vessel size imaging: a longitudinal in vivo study. Clin Cancer Res 16(12):3215–3225
36. Grankvist J et al (2012) MRI and PET/CT of patients with bone metastases from breast carcinoma. Eur J Radiol 81(1):e13–e18
37. Walkington L, Coleman RE (2011) Advances in management of bone disease in breast cancer. Bone 48(1):80–87
38. Coleman RE, McCloskey EV (2011) Bisphosphonates in oncology. Bone 49(1):71–76
39. Aapro MS, Coleman RE (2012) Bone health management in patients with breast cancer: current standards and emerging strategies. Breast 21(1):8–19
40. Eisenhauer EA et al (2009) New response evaluation criteria in solid tumours: revised RECIST guideline (version 1.1). Eur J Cancer 45(2):228–247
41. Doré-Savard L et al (2010) Behavioral, medical imaging and histological features of a new rat model of bone cancer pain. PLoS One 5(10):e13774
42. Tetreault P et al (2011) Weight bearing evaluation in inflammatory, neuropathic and cancer chronic pain in freely moving rats. Physiol Behav 104(3):495–502
43. Castaneda-Corral G et al (2011) The majority of myelinated and unmyelinated sensory nerve fibers that innervate bone express the tropomyosin receptor kinase A. Neuroscience 178:196–207
44. Mercadante S, Fulfaro F (2007) Management of painful bone metastases. Curr Opin Oncol 19(4):308–314
45. Angst MS, Clark JD (2006) Opioid-induced hyperalgesia: a qualitative systematic review. Anesthesiology 104(3):570–587
46. King T et al (2007) Morphine treatment accelerates sarcoma-induced bone pain, bone loss, and spontaneous fracture in a murine model of bone cancer. Pain 132(1–2):154–168
47. Hamaoka T et al (2004) Bone imaging in metastatic breast cancer. J Clin Oncol 22(14):2942–2953
48. Gauvain KM et al (2005) MRI detection of early bone metastases in b16 mouse melanoma models. Clin Exp Metastasis 22(5): 403–411

49. Wang L et al (2008) MRI and hybrid PET/CT for monitoring tumour metastasis in a metastatic breast cancer model in rabbit. Nucl Med Commun 29(2):137–143
50. Kundra V et al (2007) In vivo imaging of prostate cancer involving bone in a mouse model. Prostate 67(1):50–60
51. Murakami K et al (2008) Correlation between high field MR images and histopathological findings of rat transplanted cancer immediately after partial microwave coagulation. Magn Reson Med Sci 7(3):105–112
52. Reichardt W et al (2009) Diffusion-weighted imaging as predictor of therapy response in an animal model of Ewing sarcoma. Invest Radiol 44(5):298–303
53. Rozel S et al (2009) Synergy between anti-CCL2 and docetaxel as determined by DW-MRI in a metastatic bone cancer model. J Cell Biochem 107(1):58–64
54. Walker K et al (2002) Disease modifying and anti-nociceptive effects of the bisphosphonate, zoledronic acid in a model of bone cancer pain. Pain 100(3):219–229
55. Shah M et al (2012) An MMP13-selective inhibitor delays primary tumor growth and the onset of tumor-associated osteolytic lesions in experimental models of breast cancer. PLoS ONE 7(1):e29615
56. Holland PM et al (2010) Combined therapy with the RANKL inhibitor RANK-Fc and rhApo2L/TRAIL/dulanermin reduces bone lesions and skeletal tumor burden in a model of breast cancer skeletal metastasis. Cancer Biol Ther 9(7):539–550
57. Svensson CI et al (2008) Role of p38 mitogen activated protein kinase in a model of osteosarcoma-induced pain. Pharmacol Biochem Behav 90(4):664–675
58. Ghilardi JR et al (2011) Sustained blockade of neurotrophin receptors TrkA, TrkB and TrkC reduces non-malignant skeletal pain but not the maintenance of sensory and sympathetic nerve fibers. Bone 48(2):389–398
59. Mantyh WG et al (2010) Blockade of nerve sprouting and neuroma formation markedly attenuates the development of late stage cancer pain. Neuroscience 171(2):588–598
60. Peters CM et al (2005) Tumor-induced injury of primary afferent sensory nerve fibers in bone cancer pain. Exp Neurol 193(1): 85–100
61. Sevcik MA et al (2005) Anti-NGF therapy profoundly reduces bone cancer pain and the accompanying increase in markers of peripheral and central sensitization. Pain 115(1–2):128–141
62. Kaan TK et al (2010) Systemic blockade of P2X3 and P2X2/3 receptors attenuates bone cancer pain behaviour in rats. Brain 133(9):2549–2564
63. Ghilardi JR et al (2010) Administration of a tropomyosin receptor kinase inhibitor attenuates sarcoma-induced nerve sprouting, neuroma formation and bone cancer pain. Mol Pain 6:87
64. Zwolak P et al (2008) Local irradiation in combination with bevacizumab enhances radiation control of bone destruction and cancer-induced pain in a model of bone metastases. Int J Cancer 122(3):681–688
65. Hipp JA, Springfield DS, Hayes WC (1995) Predicting pathologic fracture risk in the management of metastatic bone defects. Clin Orthop Relat Res 312:120–135
66. El Mouedden M, Meert TF (2005) Evaluation of pain-related behavior, bone destruction and effectiveness of fentanyl, sufentanil, and morphine in a murine model of cancer pain. Pharmacol Biochem Behav 82(1):109–119
67. Tong Z et al (2010) Tumor tissue-derived formaldehyde and acidic microenvironment synergistically induce bone cancer pain. PLoS ONE 5(4):e10234
68. Yoneda T et al (2011) Involvement of acidic microenvironment in the pathophysiology of cancer-associated bone pain. Bone 48(1):100–105
69. Lipton A, Jacobs I (2011) Denosumab: benefits of RANK ligand inhibition in cancer patients. Curr Opin Support Palliat Care 5(3):258–264
70. Pantano F et al (2011) New targets, new drugs for metastatic bone pain: a new philosophy. Expert Opin Emerg Drugs 16(3): 403–405
71. Costa L, Major PP (2009) Effect of bisphosphonates on pain and quality of life in patients with bone metastases. Nat Clin Pract Oncol 6(3):163–174
72. Costa L et al (2011) Anticancer evidence for zoledronic acid across the cancer continuum. Crit Rev Oncol Hematol 77(Suppl 1): S31–S37
73. Zheleznyak A et al. (2011) Integrin alpha(v)beta (3) as a PET imaging biomarker for osteoclast number in mouse models of negative and positive osteoclast regulation. Mol Imaging Biol Aug 19: 1–9
74. Lage MJ et al (2008) The cost of treating skeletal-related events in patients with prostate cancer. Am J Manag Care 14(5):317–322